

**Search for the standard model Higgs boson in the $ZH \rightarrow \nu\bar{\nu}b\bar{b}$ channel
in 5.2 fb^{-1} of $p\bar{p}$ collisions at $\sqrt{s} = 1.96 \text{ TeV}$**

The DØ Collaboration

URL: <http://www-d0.fnal.gov>

(Dated: November 14, 2009)

A search for the standard model Higgs boson is performed in 5.2 fb^{-1} of $p\bar{p}$ collisions at $\sqrt{s} = 1.96 \text{ TeV}$, collected with the DØ detector at the Fermilab Tevatron. The final state considered is a pair of b jets with large missing transverse energy, as expected from $p\bar{p} \rightarrow ZH \rightarrow \nu\bar{\nu}b\bar{b}$ production. The search is also sensitive to the $WH \rightarrow \ell\nu b\bar{b}$ channel, when the charged lepton is not identified. Boosted decision trees are used to discriminate signal from background. Good agreement is observed between data and expected backgrounds. For a Higgs-boson mass of 115 GeV, a limit is set at 95% C.L. on the cross section multiplied by branching fraction for $(p\bar{p} \rightarrow (Z/W)H) \times (H \rightarrow b\bar{b})$ that is a factor 3.7 larger than the standard-model value, while the expected limit is a factor 4.6 larger.

Preliminary Results for Autumn 2009 Conferences

I. INTRODUCTION

The associated ZH production in $p\bar{p}$ collisions, with $Z \rightarrow \nu\bar{\nu}$ and $H \rightarrow b\bar{b}$, is among the most promising processes for finding evidence for a low-mass Higgs boson at the Fermilab Tevatron [1]. The DØ collaboration published a search for this process based on 0.9 fb^{-1} of data [2], and a preliminary result based on 2.1 fb^{-1} was reported more recently [3]. This note presents an extension of this search to 5.2 fb^{-1} . A lower limit of 114.4 GeV was set by the LEP experiments on the mass of the Higgs boson from analyses of the reaction $e^+e^- \rightarrow ZH$ [4], while an upper limit of 157 GeV can be inferred from precision electroweak data [5]. These limits and those to follow are all defined at 95% confidence.

The final-state topology considered in this analysis is a pair of b jets from the decay of the Higgs boson, and missing transverse energy (\cancel{E}_T) due to the two escaping neutrinos from Z decay. The search is therefore also sensitive to the WH channel, when the charged lepton from $W \rightarrow \ell\nu$ decay is not detected. The main backgrounds arise from $(W/Z)b\bar{b}$, $(W/Z)+(\text{non-}b \text{ jets})$ where light-flavor jets are misidentified as b jets (mistagged), top-quark production, e.g., $t\bar{t} \rightarrow \ell\nu b q \bar{q}' \bar{b}$ or $t(q)\bar{b} \rightarrow \ell\nu b(q)\bar{b}$, diboson production such as $WZ \rightarrow \ell\nu b\bar{b}$ or $ZZ \rightarrow \nu\bar{\nu} b\bar{b}$, and from multijet events produced via the strong interaction, containing true b jets or mistagged light-parton jets and \cancel{E}_T arising from fluctuations in measurement of jet energies.

A kinematic selection is first applied to reject most of the multijet events. Then jets expected to arise from Higgs-boson decays are required to be identified as b jets. Finally, discrimination between signal and remaining backgrounds is achieved using a boosted-decision-tree technique.

II. DATA AND SIMULATED SAMPLES

The DØ detector [6] has a central silicon microstrip vertex detector and a fiber tracker located within a 1.9 T superconducting solenoidal magnet. A liquid-argon and uranium sampling calorimeter, housed in three separate cryostats, provides pseudorapidity coverage out to $|\eta| \simeq 4.2$, and uses pseudo-projective towers of size 0.1×0.1 in (η, ϕ) , where η is calculated relative to the center of the detector, and ϕ is the azimuthal angle. The calorimeter is segmented longitudinally into four electromagnetic and up to five hadronic layers. Additional shower sampling is provided by scintillating tiles located between cryostats. Beyond the calorimeter, a muon system has tracking detectors and scintillation trigger counters before and following 1.8 T iron toroids.

Online event selection is based on a three-level trigger system. For this analysis, the data were recorded using a set of triggers designed to select events with jets and \cancel{E}_T . At the highest trigger level, the main requirement through Run IIa was $\cancel{E}_T > 30 \text{ GeV}$, where $\cancel{E}_T = |-\sum \vec{p}_{T\text{jet}}|$ is a measure of \cancel{E}_T based only on jets. For data collected during Run IIb, the trigger system was improved [7], providing \cancel{E}_T at the first level, and enabling a lower \cancel{E}_T threshold of 25 GeV. Between Runs IIa and IIb, an additional layer of silicon tracking was installed close to the beam pipe, and the quality of the calibration of the scintillating tiles was greatly improved.

After imposing data quality requirements, a total integrated luminosity [8] of $(5.16 \pm 0.32) \text{ fb}^{-1}$ was available, 82% of which was collected during Run IIb. This analysis relies on charged particle tracks, the primary interaction vertex, calorimeter jets reconstructed in a cone of radius 0.5, using the iterative midpoint cone algorithm [9], accepting jets with $p_T > 15 \text{ GeV}$, electrons or muons identified through an association of charged particles with electromagnetic calorimeter clusters or with hits in the muon detector, respectively. The \cancel{E}_T is reconstructed as the opposite of the vectorial sum of transverse energies of all energy depositions in the calorimeter and, unless specified to the contrary, it is corrected for reconstructed muons. Jet energies are calibrated through imposition of transverse energy balance in photon+jet events, and this calibration is also propagated to \cancel{E}_T .

Except for background from multijet production, which is estimated from data, all backgrounds from standard-model (SM) processes are determined through Monte Carlo simulation. The $(W/Z)+\text{jets}$ processes are generated with ALPGEN [10], interfaced to PYTHIA [11] for initial and final-state gluon radiation and parton hadronization. A matching algorithm [12] is applied to avoid double counting in regions of phase space populated by both ALPGEN and PYTHIA. Light (u, d, s, g) and heavy (c, b) flavor production in association with W/Z are generated separately, and double counting of events containing heavy-flavor jets produced directly in ALPGEN or in PYTHIA is avoided. The p_T spectrum of the Z is reweighted so as to match the DØ measurement [13]. The p_T spectrum of the W is reweighted using the same experimental input, corrected for the differences between the Z and W p_T spectra predicted in next-to-next-to-leading order (NNLO) QCD [14]. For $t\bar{t}$ and for electroweak single-top production, the ALPGEN and COMPHEP [15] generators, respectively, are interfaced with PYTHIA, while vector-boson pair-production processes are generated with PYTHIA. The signal (ZH and WH) is generated with PYTHIA for Higgs-boson masses (m_H) ranging from 100 to 150 GeV, in 5 GeV steps. All these simulations use CTEQ6L1 parton distribution functions (PDFs) [16].

For the $(W/Z)+\text{jets}$ processes, absolute normalizations are obtained from NNLO calculations of the total cross sections based on Ref. [17], using the MRST2004 NNLO PDFs [18]. The heavy-flavor fractions are obtained using

MCFM [19]. Cross sections for other background processes are taken from Refs. [20], or calculated with MCFM, and the cross sections for signal are taken from Ref. [21].

Signal and background samples are passed through full GEANT3-based simulation [22] of detector geometry and response, and processed with the same reconstruction program as used for data. Events from randomly selected beam crossings are overlaid on simulated events to account for detector noise and additional contributions from minimum-bias interactions. The trigger conditions on jets and \cancel{E}_T are not included in the simulation, but parameterizations of trigger efficiency are applied, as determined from triggers based only on information from the muon detectors, and therefore independent of those used in this analysis. Weight factors are applied to compensate for residual differences between data and simulation in luminosity profile, longitudinal distribution of the primary vertex, and electron, muon and jet identification. The jet energy calibration and resolution are adjusted in simulated events so as to match those measured in data.

III. EVENT SELECTION

The initial preselection criteria are meant to largely reduce the overwhelming background from multijet events, but retain high efficiency for signal. At a second stage, enhancement of sensitivity is achieved using b tagging, with the analysis optimized for a Higgs-boson mass of 115 GeV.

The primary vertex (PV) must be reconstructed within the acceptance of the silicon vertex detector ($|z_{\text{PV}}| < 40$ cm, where z is measured from the center of the detector along the beam direction), and at least three charged particle tracks have to originate from that vertex. Only jets with $p_T > 15$ GeV and within $|\eta| < 3.2$ are considered in the analysis, and are ordered in decreasing p_T . Jets with associated charged particle tracks (using only tracks that meet minimal quality criteria to assure that the b -tagging algorithm operates efficiently) are denoted as “taggable” jets. The event must have two or three taggable jets, one of which is the leading jet. These jets must have $p_T > 20$ GeV and $|\eta| < 2.5$. A large fraction of multijet events is rejected by requiring that the two leading taggable jets are not back-to-back in the plane transverse to the beam direction: $\Delta\phi(\text{jet}_1, \text{jet}_2) < 165^\circ$. Finally, $\cancel{E}_T > 20$ GeV is required for accepting the event.

After these preselection requirements, additional criteria are used to define four distinct samples: *i*) an analysis sample used to search for a Higgs-boson signal, *ii*) an electroweak (EW) control sample, enriched in $(W \rightarrow \mu\nu) + \text{jets}$ events, where the jet system has a topology similar to that of the analysis sample, and used to validate the SM-background simulation, *iii*) an “MJ-model” sample, dominated by multijet events, and used to model the multijet background in the analysis sample, and *iv*) a large multijet control sample, used to validate the MJ-modeling procedure.

To select the analysis sample, the threshold on \cancel{E}_T is increased to 40 GeV. The multijet background can be reduced using the “ \cancel{E}_T significance” \mathcal{S} . This variable takes into account the resolution of jet energies to assess the significance of the observed \cancel{E}_T relative to expected fluctuations in measured jet energies. The larger the \mathcal{S} , the more likely it is that the observed \cancel{E}_T is not due to such fluctuations. A value of \mathcal{S} larger than 5 is required. For signal, the missing track p_T , \not{p}_T , defined as the opposite of the vectorial sum of the charged particle transverse momenta, is expected to point in a direction close to that of \cancel{E}_T . This is not expected in multijet events, in which the \cancel{E}_T originates mainly from mismeasurements of jet energies. Advantage is taken of this feature by requiring $\mathcal{D} < \pi/2$, where $\mathcal{D} = \Delta\phi(\cancel{E}_T, \not{p}_T)$. To reject backgrounds from $W + \text{jets}$, top, and diboson production, events containing an isolated electron or muon are rejected. To keep this analysis orthogonal to the searches in the $WH \rightarrow \ell\nu b\bar{b}$ channels, electrons and muons are identified as in Ref. [23]. Additional criteria are applied to Run IIa data to mimic the more selective trigger conditions of Run IIb: the uncorrected \cancel{E}_T must exceed 30 GeV, and the direction of the \cancel{E}_T must not be too close to the direction of any of the jets in the plane transverse to the beam direction, $\cancel{E}_T(\text{GeV}) > 80 - 40 \times \min\Delta\phi(\cancel{E}_T, \text{any jet})$ (referred to as the “triangle cut”), where the angle is measured in radians.

The EW-control sample is selected in a way similar to the analysis sample, except that the muon veto is not implemented, and instead a muon (the “W-muon”) with $p_T > 15$ GeV is required within $|\eta| < 2$. The multijet content of this sample is rendered negligible by the requirements of $\cancel{E}_T > 20$ GeV and of a large transverse mass for the muon and \cancel{E}_T system, $m_T > 30$ GeV. To ensure similar jet topologies in the analysis and EW-control samples, the \cancel{E}_T that is not corrected for the W-muon is required to exceed 40 GeV.

The variable \mathcal{D} is used to define the MJ-model sample. It is selected in the same way as the analysis sample, except that the previous requirement $\mathcal{D} < \pi/2$ is now inverted. The small contribution from SM processes in that $\mathcal{D} > \pi/2$ region is subtracted, and the resulting sample is used to model multijet background in the analysis sample, i.e., in the $\mathcal{D} < \pi/2$ region. After adding the contributions from SM backgrounds, the multijet background is normalized so that the expected number of events is identical to the number observed in the analysis sample, i.e., in the $\mathcal{D} < \pi/2$ region.

The multijet control sample is used to test the validity of this approach. It is defined in the same way as the analysis sample, except that the \cancel{E}_T threshold is reduced to 30 GeV and no requirement is imposed on \mathcal{S} . The triangle cut for

Run IIa data is also removed. As a result, multijet events largely dominate not only the $\mathcal{D} > \pi/2$ region, but also the $\mathcal{D} < \pi/2$ region. This sample is then used to verify how well the events with $\mathcal{D} > \pi/2$ model those with $\mathcal{D} < \pi/2$.

Examples of distributions for the EW-control sample before b tagging are given in Fig. 1(a,b). Here and in the following, the dijet mass is calculated from the two leading taggable jets. The number of selected events is found to be in excellent agreement with the expectation based on the (W/Z) +jets initial normalization. Analogous distributions for the multijet control sample are shown in Fig. 1(c,d).

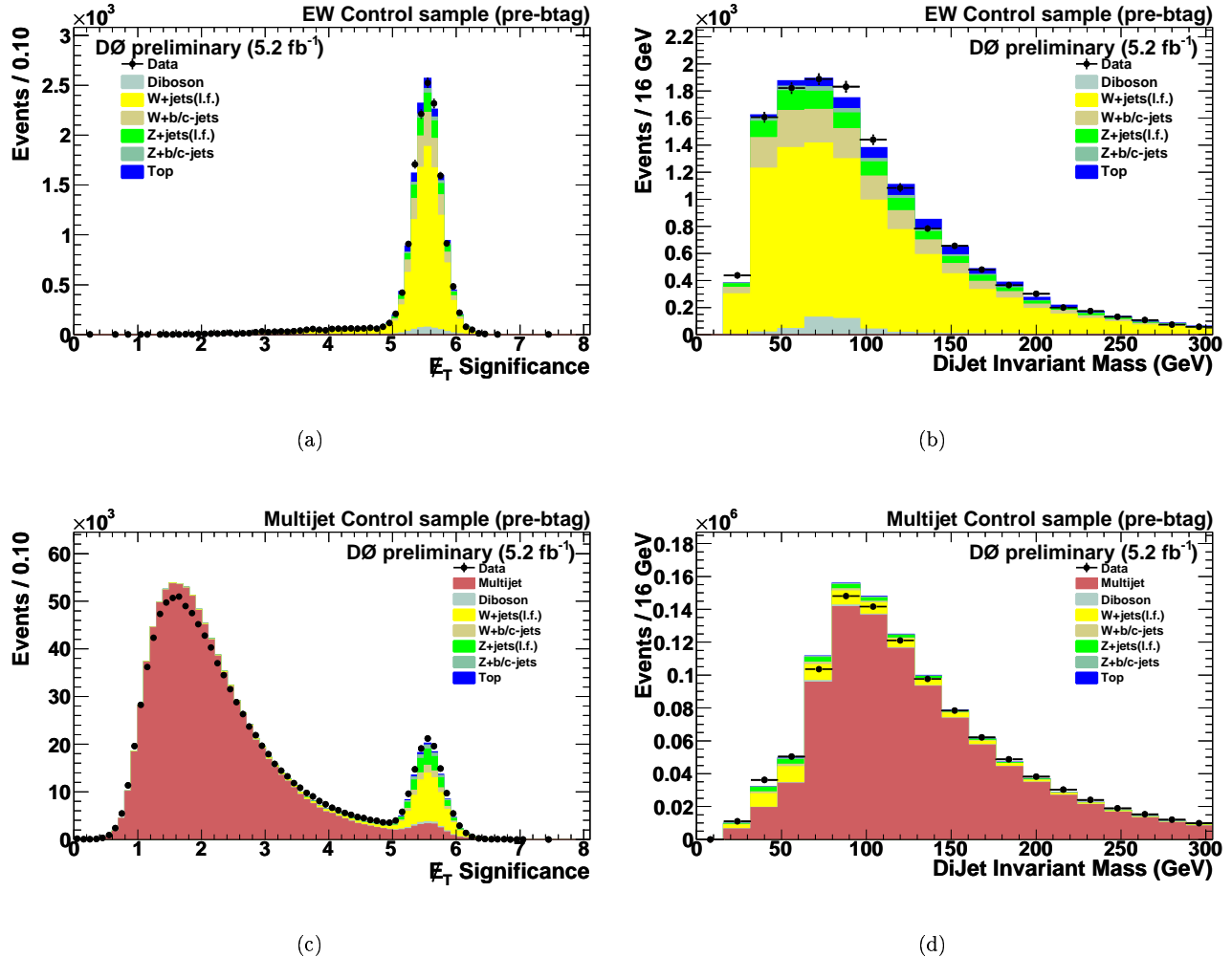


FIG. 1: Distributions in E_T significance are given in (a,c), and in dijet mass in (b,d), all before b tagging. The EW-control sample is used in (a,b), and the multijet control sample in (c,d). In (a,b), the data are shown as points with error bars, and the SM background contributions as histograms; the MJ background is negligible in the EW-control sample. In (c,d), the data for $\mathcal{D} < \pi/2$ are shown as points with error bars; the multijet background prediction from events with $\mathcal{D} > \pi/2$ and the small SM background contributions are shown as histograms. Color codes are indicated in the legends. The $\mathcal{S} > 5$ requirement is not implemented in (a,c,d).

Distributions for the analysis sample are shown in Fig. 2. The combination of multijet events from the MJ-model sample and simulated SM backgrounds provides a good description of the shapes of the data.

Advantage is next taken of the large branching fraction for $H \rightarrow b\bar{b}$ by requiring that one or both of the two leading taggable jets be b tagged. The double-tag sample is selected with asymmetric requirements on the outputs of a b -tagging neural-network algorithm [24], such that one jet is tagged with an efficiency of $\sim 70\%$ (“loose tag”), and the other with an efficiency of $\sim 50\%$ (“tight tag”). These values apply to taggable jets with $p_T \sim 45$ GeV and $|\eta| \sim 0.8$. The corresponding mistag rates, i.e., the probabilities to tag u, d, s, g jets as b jets, are $\sim 6.5\%$ and $\sim 0.5\%$, respectively. This asymmetric tagging procedure is found to provide the best sensitivity to a Higgs-boson signal. To enhance the sensitivity of the search, an independent data sample is defined that has one of the two

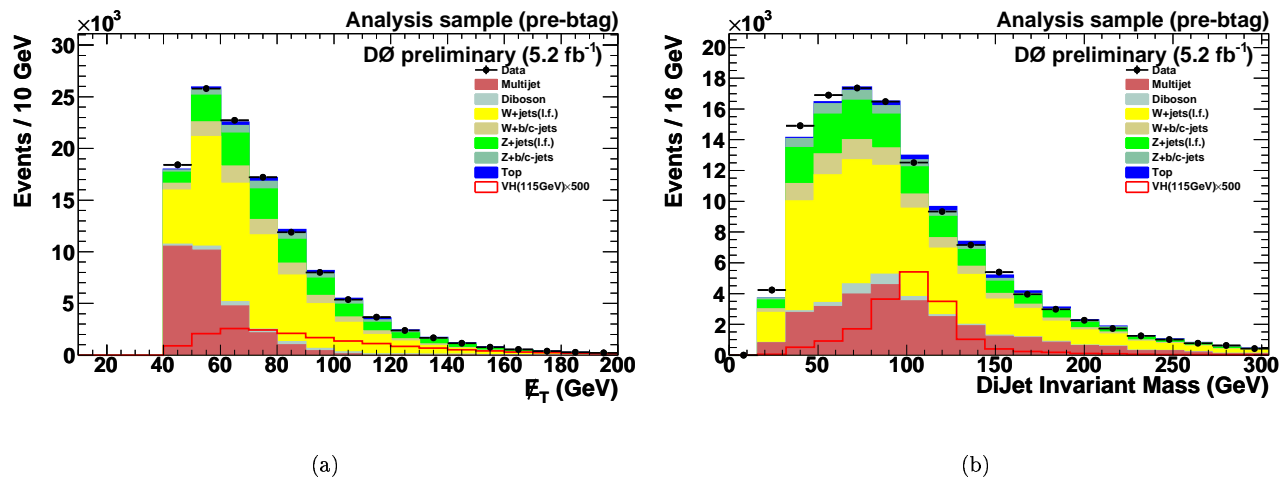


FIG. 2: Distributions for the analysis sample before b tagging: (a) \cancel{E}_T , and (b) dijet mass. The data are shown as points with error bars. The background contributions (SM and multijet) are shown as histograms, with color codes indicated in the legends. Distributions for a signal with $m_H = 115$ GeV are shown multiplied by 500.

leading taggable jets passing the tight tag, and the other one failing the loose tag. In the following, this sample is denoted the single-tag sample. Finally, the complementary sample, in which neither of the leading taggable jets passes the tight tag, is called the 0-tag sample. To correct for differences in track reconstruction efficiencies for data and simulation, flavor-dependent scale factors measured in dedicated data samples are applied to b -tagging efficiencies in the simulation. The normalizations of the MJ-model with single and double b tags are adjusted to get the same enhancement factors from b tagging as found in the multijet control sample.

From the numbers of 0-tag, single-tag, and double-tag events in the EW-control sample, a scale factor can be calculated for the heavy-flavor fraction in (W/Z) +jets events. This factor is found to be 1.05 ± 0.10 , in good agreement with the expected value of unity. This factor is applied throughout the analysis, except when extracting the final results, because the EW-control sample is subject to possible signal contamination.

The effect of b tagging on the EW-control and multijet control samples can be seen in Fig. 3.

IV. ANALYSIS USING DECISION TREES

A boosted-decision-tree technique [25] is used to take advantage of the different kinematics for signal and background processes. For each assumed m_H , the decision tree (DT) training is performed for ten boosting cycles on one third of the signal and background samples, with the remaining events used to extract results.

For each m_H , an “MJR DT” (multijet-rejection DT) used to discriminate between signal and MJ-model events is trained at the pretag level. A total of 23 kinematic variables are used, including the number of jets, jet $p_{T\text{S}}$, \cancel{E}_T , angles between jets and between jets and \cancel{E}_T , number of isolated charged-particle tracks, and the dijet mass. The MJR DT output (multijet discriminant) is shown in Fig. 4(a) for $m_H = 115$ GeV. Requiring a value of this multijet discriminant in excess of 0.6 (multijet veto) removes over 95% of the multijet background and 65% of the other backgrounds, while retaining 70% of the signal. Details of the numbers of expected signal and background events, as well as the numbers of observed events, are given in Table I, after requiring that the multijet discriminant be greater than 0.6. At all b -tagging levels, the numbers of observed events are consistent with the numbers expected from backgrounds, once the systematic uncertainties discussed below are taken into account. After imposing double b tagging, about 90% of the (W/Z) +jets background is from heavy-flavor production. Distributions after requiring a multijet discriminant larger than 0.6 are shown in Fig. 4(b-f): dijet mass at pretag (b), single (e) and double-tag (f) levels; jet multiplicity (c) and ΔR (d) at pretag level, where $\Delta R = \sqrt{\Delta\eta^2 + \Delta\phi^2}$ is the distance in $\eta - \phi$ space between the two leading taggable jets. This same cutoff on the multijet discriminant is used for all Higgs-boson masses.

Additional “SMR DTs” (standard-model rejection DTs) are trained separately, prior to the multijet veto, at the single and double b -tag levels to discriminate signal from the other SM backgrounds. The same kinematic variables are used as for the MJR DT. The outputs of the SMR DTs (final discriminants) are shown for the analysis sample in Fig. 5 for $m_H = 115$ GeV, for the single and double b -tag samples.

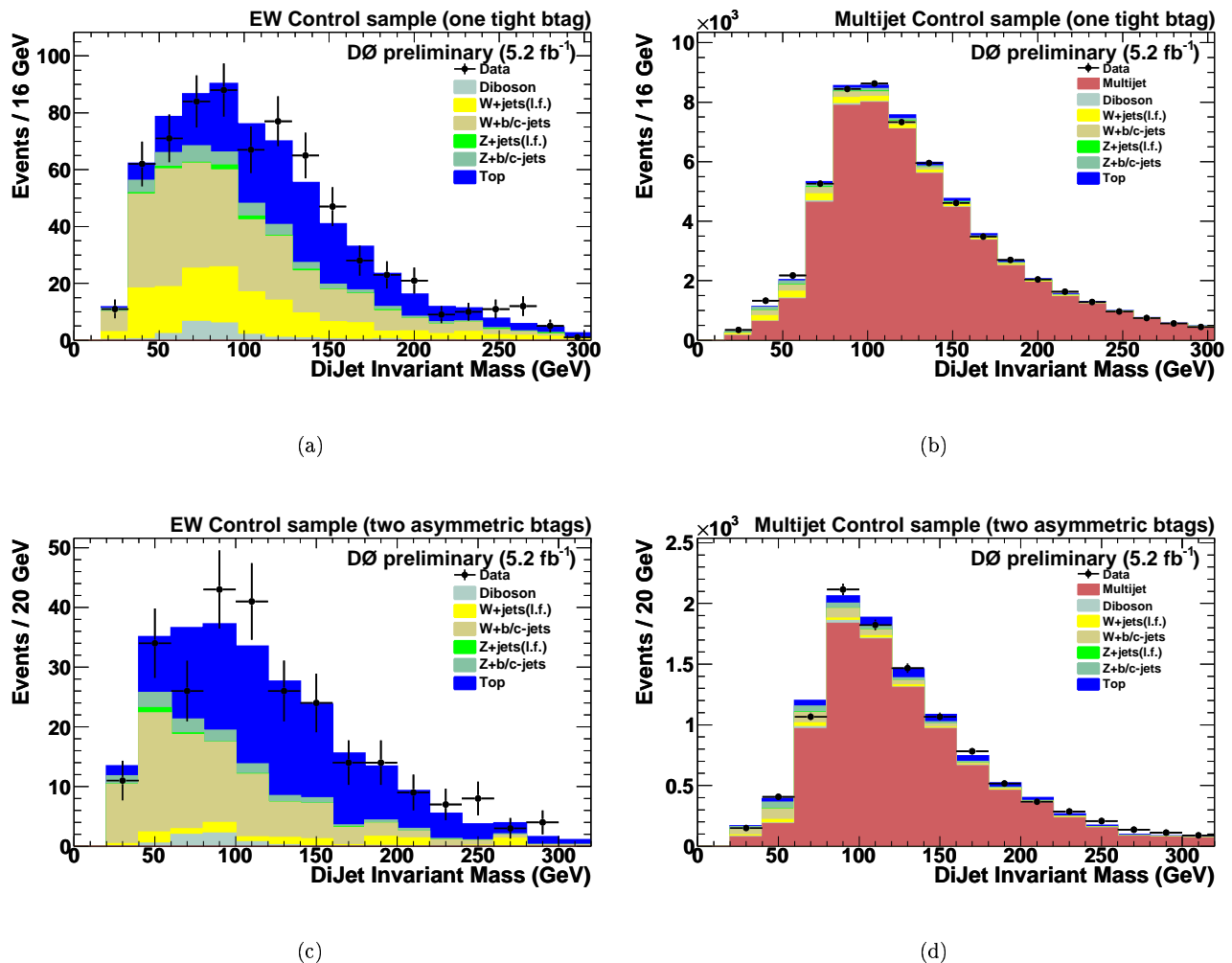


FIG. 3: Distributions in dijet mass are given in (a,b) for single b tags, and in (c,d) for double b tags. The EW-control sample is used in (a,c), and the multijet control sample in (b,d). In (a,c), the data are shown as points with error bars, and the SM background contributions as histograms. In (b,d), the data for $\mathcal{D} < \pi/2$ are shown as points with error bars, and the small SM background contributions as histograms, along with the prediction from events with $\mathcal{D} > \pi/2$. Color codes are indicated in the legends.

V. LIMIT SETTING PROCEDURE

Agreement between data and expectation from SM and multijet backgrounds is observed both in numbers of selected events (Table I) and in distributions of final discriminants (Fig. 5). A modified frequentist approach [26] is used to set limits on the cross section for SM Higgs-boson production, where the signal confidence level CL_s , defined as the ratio of confidence levels for the signal+background hypothesis to the background-only hypothesis ($CL_s = CL_{s+b}/CL_b$), is calculated by integrating distributions of a test statistic over the outcomes of pseudo-experiments, generated by Monte Carlo (MC) according to Poisson statistics, for both hypotheses. The test statistic is calculated as a joint log-likelihood ratio (LLR) obtained by summing LLR values over the bins of the final discriminants shown in Fig. 5(a,b).

The systematic uncertainties detailed below are incorporated via Gaussian smearing of the Poisson probability distributions of signal and background contributions within the MC generated ensembles of pseudo-experiments. Appropriate correlations are maintained among signal and backgrounds. To reduce the impact of systematic uncertainties on the sensitivity of the analysis, the individual signal and background contributions are fitted to data (and pseudo data) separately for the signal+background and the background-only hypotheses, by maximizing a profile likelihood function for each hypothesis [27]. The profile likelihood is constructed via a joint Poisson probability over the number of bins in the calculation, and is a function of “nuisance” parameters in the system and their uncertainties, which are

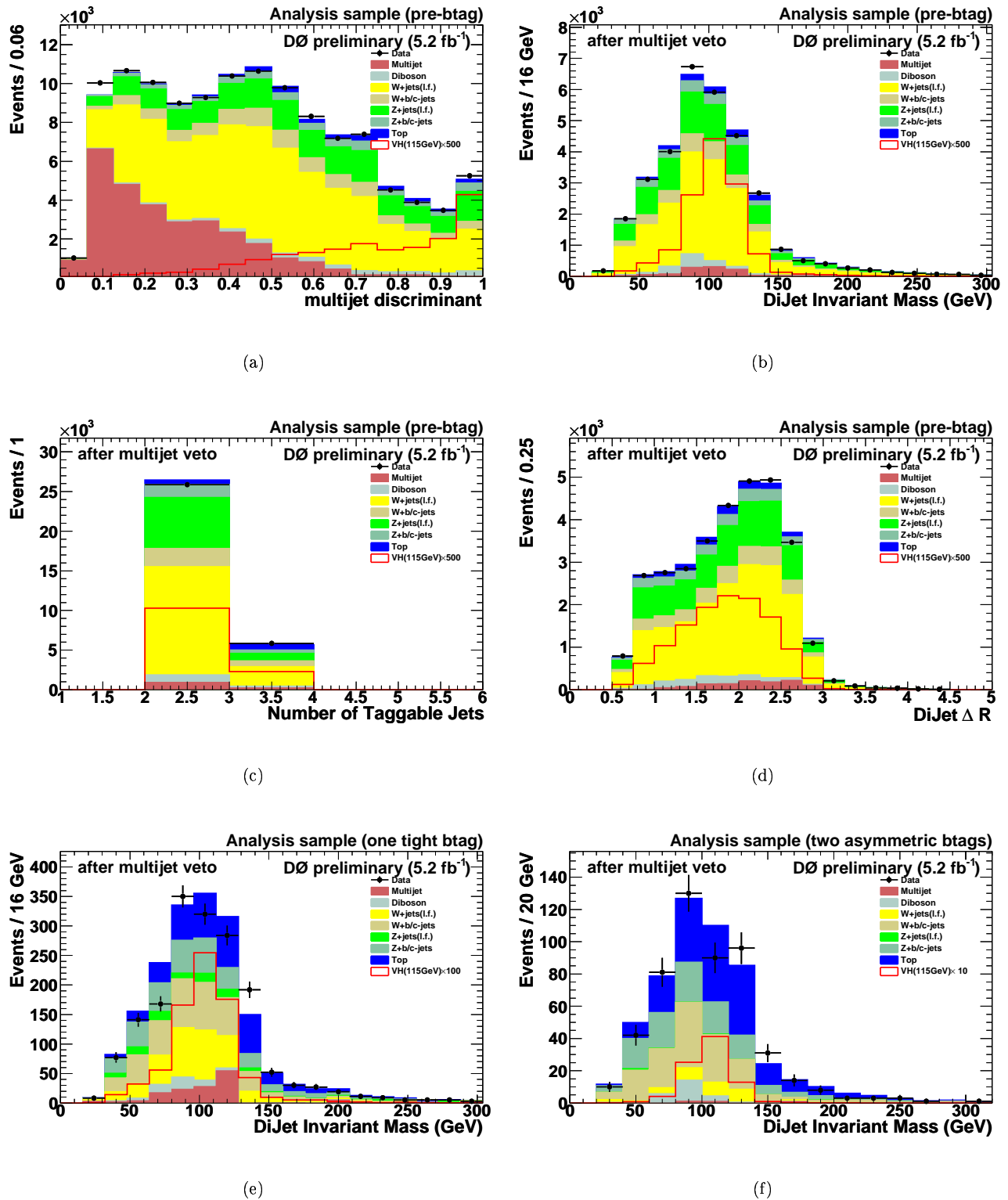


FIG. 4: Results of the MJR decision tree for $m_H = 115$ GeV: (a) multijet discriminant, (b) dijet mass before b tagging, (c) jet multiplicity before b tagging, (d) dijet ΔR before b tagging, (e) dijet mass for single b tags, (f) dijet mass for double b tags. In all distributions except (a), the multijet discriminant is > 0.6 . The data are shown as points with error bars. The background contributions (SM and multijet) are shown as histograms, with color codes indicated in the legends. The distributions for signal are shown multiplied by 500 in (a-d), by 100 in (e), and by 10 in (f).

TABLE I: In the analysis sample, expected numbers of signal and background events, and numbers of events observed after requiring a multijet discriminant larger than 0.6. These numbers of events are given prior to b tagging, as well as for single and double b tags. The signal corresponds to $m_H = 115$ GeV, “top” includes pair and single-top production, and VV stands for the sum of all diboson processes. The quoted uncertainties reflect only the statistics of the simulation. The total background is normalized to data at the pretag level, before the restriction on the multijet discriminant.

Sample	ZH	WH	W +jets	Z +jets	top	VV	multijet	Total	Observed
pretag	13.59 ± 0.08	11.55 ± 0.12	19 155	9 465	1 223	1 102	1 180	$32\,125 \pm 163$	31 718
1-tag	4.12 ± 0.05	3.58 ± 0.07	797	433	406	60	127	$1\,821 \pm 38$	1 712
2-tags	4.62 ± 0.04	3.96 ± 0.06	185	122	200	24	0^{+8}_0	530 ± 11	514

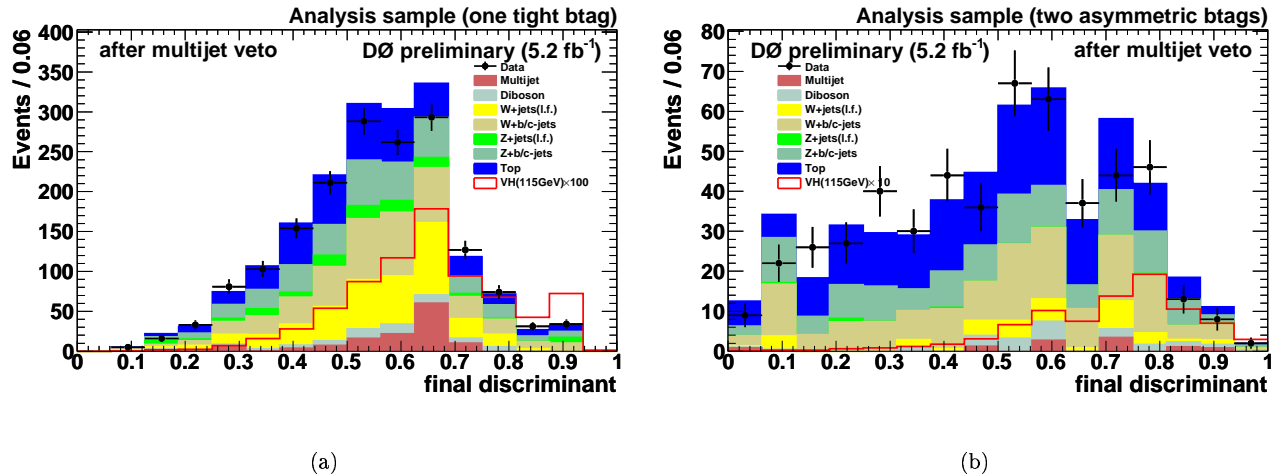


FIG. 5: Final discriminants for $m_H = 115$ GeV with (a) single, and (b) double b tags. The data are shown as points with error bars. The background contributions (SM and multijet) are shown as histograms, with color codes indicated in the legends. The distributions for signal are multiplied by a factor of 100 in (a) and 10 in (b).

given additional Gaussian constraints associated with their priors.

VI. SYSTEMATIC UNCERTAINTIES

Systematic uncertainties originate from a variety of sources. Experimental uncertainties arise from trigger simulation, jet energy calibration and resolution, jet reconstruction efficiency, lepton identification, and b tagging. The corresponding parameterizations applied to the simulation are varied within their uncertainties, and the impact assessed on both the overall normalizations and shapes of distributions in final discriminants. Correlations among systematic uncertainties in signal and background processes are taken into account in extracting the final results, including the uncertainty on the integrated luminosity of the data sample. The experimental systematic uncertainties affecting the normalizations of signal and SM background are listed in Table II.

The input cross sections for SM processes suffer from theoretical uncertainties. For (W/Z) +jets production, an uncertainty of 6% is assigned to the production cross sections, and an uncertainty of 20% on the heavy-flavor fractions is estimated using MCFM. For other background processes, theoretical uncertainties are taken from Refs. [20] or from MCFM, and range from 6% to 10%. The uncertainties on cross sections for signal (6% for $m_H = 115$ GeV) are taken from Ref. [21]. Uncertainties on the modeling of (W/Z) +jets events are assessed by varying the renormalization-and-factorization scale, and by comparing ALPGEN interfaced with HERWIG [28] to ALPGEN interfaced with PYTHIA. Uncertainties on signal and background acceptances due to the choice of PDF are estimated using the forty-eigenvector basis of the CTEQ6.1M PDF set [16].

The normalization of the multijet background at the pretag level is anticorrelated with the normalization of the other SM backgrounds, as the sum is constrained by data prior to b tagging. In the b -tagged samples, however, the normalization uncertainties are such that these normalizations are allowed to vary freely in the limit setting.

TABLE II: Experimental systematic uncertainties (in %) on predicted signal (for $m_H = 115$ GeV) and SM backgrounds for: integrated luminosity (Lumi), trigger efficiency, jet energy calibration (J-C), jet energy resolution (J-R), jet reconstruction efficiency (J-E), lepton identification (ℓ), and b tagging. These uncertainties apply to the double tag samples.

	Lumi	Trigger	J-C	J-R	J-E	ℓ	b tagging
Signal	6.1	3.5	2.7	0.9	4.5	1.1	8.7
SM backgrounds	6.1	3.4	3.5	0.8	3.7	1.6	7.9

TABLE III: As a function of m_H , observed and expected ratios of excluded to SM production cross sections multiplied by branching fractions for $H \rightarrow b\bar{b}$.

mass	100	105	110	115	120	125	130	135	140	145	150
observed	3.7	4.0	3.2	3.7	4.6	5.6	8.2	14.5	15.3	24.4	43.6
expected	3.5	3.7	4.2	4.6	5.4	6.3	7.6	10.5	14.0	20.5	32.3

VII. RESULTS

The results of limit setting are shown as a function of m_H in Fig. 6 and in Table III, in terms of the ratio of excluded cross section to the SM-expected production cross section multiplied by branching fraction for $H \rightarrow b\bar{b}$. The LLRs are also shown in Fig. 6. The observed limit is in agreement with the expected limit, defined as the median of the limits obtained in background-only pseudo experiments. For a 115 GeV Higgs-boson mass, the observed and expected limits on the combined cross section of ZH and WH production multiplied by the branching fraction for $H \rightarrow b\bar{b}$ are factors of 3.7 and 4.6 larger than the SM value, respectively.

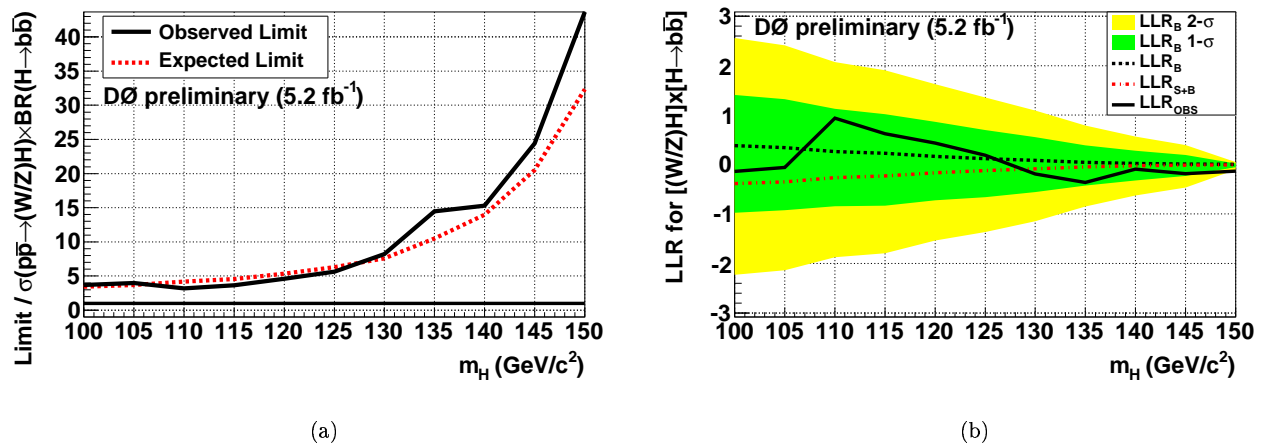


FIG. 6: In (a), the limit on the cross section for combined ZH and WH production multiplied by the branching fraction for $H \rightarrow b\bar{b}$, relative to its standard-model value, and in (b) the log likelihood ratio, both results displayed as a function of m_H . In (a), the observed and expected limits are shown as solid and dashed curves, respectively. In (b), the observed LLR is shown as a solid curve, the expected LLRs are shown as black and red dashed curves for the background-only and signal+background hypotheses, respectively, and the green and yellow areas correspond to the one and two standard deviations around the expected LLR for background-only. A Higgs-boson signal would appear as a significant negative excursion of the LLR.

VIII. SUMMARY

A search for the standard-model Higgs boson was performed in 5.2 fb⁻¹ of $p\bar{p}$ collisions at $\sqrt{s} = 1.96$ TeV. The topology analyzed consists of a pair of b jets with large \cancel{E}_T , as expected from $p\bar{p} \rightarrow ZH \rightarrow \nu\bar{\nu}b\bar{b}$. The search is also sensitive to WH production, when the W decays leptonically and the charged lepton is not detected. With no deviation observed from expectation from standard model backgrounds, outputs of boosted decision trees were used

to extract an upper limit on the cross section for the combined $p\bar{p} \rightarrow ZH$ and $p\bar{p} \rightarrow WH$ processes, as a function of the Higgs-boson mass. For a mass of 115 GeV, the observed (expected) limit is a factor 3.7 (4.6) larger than the standard-model cross section.

-
- [1] M. Carena *et al.*, “Report of the Tevatron Higgs Working Group”, arXiv:hep-ph/0010338; CDF and DØ Collaborations, “Results of the Tevatron Higgs Sensitivity Study”, FERMILAB-PUB-03/320-E (2003).
- [2] V.M. Abazov *et al.* (DØ Collaboration), Phys. Rev. Lett. **101**, 251802 (2008).
- [3] The DØ Collaboration, “Search for the standard model Higgs boson in the $HZ \rightarrow b\bar{b}\nu\bar{\nu}$ channel in 2.1 fb⁻¹ of $p\bar{p}$ collisions at $\sqrt{s} = 1.96$ TeV”, DØ Note 5586-CONF (2008).
- [4] R. Barate *et al.* [LEP Working Group for Higgs boson searches], Phys. Lett. B **565**, 61 (2003).
- [5] The LEP Electroweak Working Group, “Status of August 2009”, <http://lepewwg.web.cern.ch/LEPEWWG/>.
- [6] V.M. Abazov *et al.* (DØ Collaboration), Nucl. Instrum. Methods in Phys. Res. A **565**, 463 (2006).
- [7] M. Abolins *et al.*, Nucl. Instrum. Methods in Phys. Res. A **584/1**, 75 (2007).
- [8] T. Andeen *et al.*, “The DØ experiment’s integrated luminosity for Tevatron Run IIa”, FERMILAB-TM-2365 (2007).
- [9] G.C. Blazey *et al.*, in *Proceedings of the Workshop: “QCD and Weak Boson Physics in Run II”*, edited by U. Baur, R.K. Ellis, and D. Zeppenfeld (Fermilab, Batavia, IL, 2000), p.47; see Sec. 3.5 for details.
- [10] M.L. Mangano *et al.*, JHEP **0307**, 001 (2003); version 2.11 was used.
- [11] T. Sjöstrand, S. Mrenna and P. Skands, JHEP **0605**, 026 (2006); version 6.409 was used.
- [12] S. Höche *et al.*, “Matching Parton Showers and Matrix Elements”, in *Proceedings of the Workshop on the Implications of HERA for LHC Physics*, ed. A. De Roeck and H. Jung (CERN, Geneva, 2005), p288.
- [13] V.M. Abazov *et al.* (DØ Collaboration), Phys. Rev. Lett. **100**, 102002 (2008).
- [14] K. Melnikov and F. Petriello, Phys. Rev. **D74**, 114017 (2006).
- [15] E. Boos *et al.* (CompHEP Collaboration), Nucl. Instrum. Methods in Phys. Res. A **534**, 250 (2004).
- [16] J. Pumplin *et al.*, JHEP **0207**, 012 (2002); D. Stump *et al.*, JHEP **0310**, 046 (2003).
- [17] R. Hamberg, W.L. van Neerven, and W.B. Kilgore, Nucl. Phys. **B359**, 343 (1991), and erratum in **B644**, 403.
- [18] A.D. Martin, R.G. Roberts, W.J. Stirling, and R.S. Thorne, Phys. Lett. **B604**, 61 (2004).
- [19] J.M. Campbell and R.K. Ellis, Phys. Rev. D **60**, 113006 (1999).
- [20] M. Cacciari *et al.*, JHEP **404**, 068 (2004); N. Kidonakis and R. Vogt, Phys. Rev. D **68**, 114014 (2003); N. Kidonakis, Phys. Rev. D **74**, 114012 (2006).
- [21] T. Hahn *et al.*, “SM and MSSM Higgs Boson Production Cross Sections at the Tevatron and the LHC”, arXiv:hep/ph:0607308v2.
- [22] R. Brun and F. Carminati, CERN Program Library Long Writeup W5013, 1993 (unpublished).
- [23] The DØ Collaboration, “Search for WH associated production using neural networks with 5.0 fb⁻¹ of Tevatron data”, DØ Note 5972-CONF (2009).
- [24] T. Scanlon, “b-Tagging and the Search for Neutral Supersymmetric Higgs Bosons at DØ”, FERMILAB-THESIS-2006-43.
- [25] L. Breiman *et al.*, “Classification and Regression Trees”, Wadsworth (1984); Y. Freund and R.E. Schapire, “Experiments with a new boosting algorithm”, in *Machine Learning: Proceedings of the Thirteenth International Conference*, pp. 148-156 (1996); V.M. Abazov *et al.*, Phys. Rev. Lett. **98**, 181802 (2007).
- [26] T. Junk, Nucl. Instrum. Methods in Phys. Res. A **434**, 435 (1999); A. Read, in “1st Workshop on Confidence Limits”, CERN Report No. CERN-2000-005, 2000.
- [27] W. Fisher, “Systematics and limit calculations”, FERMILAB-TM-2386-E (2006).
- [28] G. Corcella *et al.*, JHEP **0101**, 010 (2001).